Astron. Astrophys. 239, 369–374 (1990)

ASTRONOMY AND ASTROPHYSICS

A Neck-Line Structure in the dust tail of the Great January Comet 1910I

L. Pansecchi [1,⋆] **and M. Fulle** [2]

[1] Osservatorio Astronomico di Brera, Via Brera 28, I-20121 Milano, Italy
[2] Osservatorio Astronomico, Via Tiepolo 11, I-34131 Trieste, Italy

Received October 23, 1989; accepted May 22, 1990

Abstract. We analyse two anomalous structures observed in the dust tail images of C/1910I obtained by Lampland (1912), namely a strong streamer and a short, wide and real antitail. The favourable perspective of these observations allows us to exclude the possibility that the streamer is an ion ray or the result of a synchronic pile-up phenomenon, whereas the Neck-Line Structure (NLS) model (Pansecchi et al. 1987) explains these features. Numerical simulations show that the residual differences between the observations and the predictions of the NLS model are due to the very high Earth latitude on the comet orbital plane. Under these conditions, the luminosity scattered by the NLS is also strongly influenced by the collapsing dust. Moreover we show that the length of the real antitail offers a simple constraint upon hydrodynamic models of the dust-gas interactions.

Key words: comets

1. Introduction

Kimura & Liu (1977) defined "the Neck-Line" as the line connecting the second nodes of the orbital trajectories of the dust grains composing a cometary dust tail. Pansecchi et al. (1987) showed that the concentration of dust along such a line can generate a streamer superimposed upon the main dust tail and a short, real antitail, lying inside the comet orbit with respect to the Sun. Such anomalous structures, named Neck-Line Structures (NLS), were identified in the dust tails of comets Bennett 1970II (Pansecchi et al. 1987) and Halley 1986III (Fulle 1987), and their photometrical analysis has yielded new information concerning the size distribution and the ejection velocity of the cometary dust (Fulle & Sedmak 1988; Cremonese & Fulle 1989). For particular observing geometries, the streamer appears to be directed towards the Sun, building up a prominent antitail in perspective. Kimura & Liu (1977) recognized a sunward Neck-Line in the antitail of Comet Arend-Roland 1957III, and Richter & Keller (1988) analysed the sunward Neck-Line of Comet Kohoutek 1973XII by means of a model similar to the NLS one.

Send offprint requests to: M. Fulle

⋆ Guest scientist

Since the Neck-Line Structures are thin layers of dust placed in the comet orbital plane, they are better detectable when the Earth latitude on the comet orbital plane λ is very low. However, due to the extreme perspective conditions of the observations of C/1970II and C/1986III ($0° < \lambda < 4°$), it was impossible to exclude completely an explanation of the observed streamer in terms of synchronic pile-up (Sekanina 1974). Moreover, when the Earth is close to the comet orbital plane, a NLS shows very small aberration angles, so that the contamination of the images by plasma rays cannot be excluded. Therefore, observations of a NLS with the Earth well away from the orbital plane of the comet would offer the opportunity both to exclude any plasma contamination, and to determine precisely the position of the streamer in the orbital plane of the comet, thus allowing one to discriminate between the synchronic and the NLS models.

Lampland (1912) obtained wide-field photographs of the tail of the Great January Comet 1910I at the Lowell Observatory which show anomalous dust structures strongly resembling an NLS. He observed a streamer south of the main dust tail (the South Branch), and a short, sunward tail, $\approx 10'$ long, lying inside the orbit of the comet, so that it cannot be explained by perspective. The streamer showed large aberration angles ($PA_{RV} - PA_{SB}$, see Table 1), because the Earth was far from the comet orbital plane (λ values in Table 1), thus offering a good test for the NLS model. In this paper we check whether the anomalous dust structures of C/1910I are consistent with such a model, whether an NLS can also be observed when the Earth is far from the comet orbital plane, and which influences on the photometrical behaviour can be induced by the different perspective conditions with respect to the observations of the NLS's of C/1970II and C/1986III.

2. The observations compared to the NLS model

The geometrical data of the observations are reported in Table 1, whereas the observing geometry is sketched in Fig. 1. Partial and enlarged reproductions of the three best exposures from Lampland's (1912) published images are shown in Fig. 2. In these images the streamer is the south edge of the dust tail, and the sunward spike is visible as a faint and broad antitail. Unfortunately the original plates were not available, so that we are forced to show screened reproductions where the sunward spike is hardly

Table 1. Parameters of the observations. No.: Lowell Observatory plate classification number. UT: time of mid-exposure, Jan 1910. Δ, r: Earth-Comet and Sun-Comet distances (AU). λ: cometocentric Earth latitude on the comet orbit plane. v: Comet orbital true anomaly. PA_{RV}: Position angle of the prolonged projected radius vector. PA_{SB}: Position angle of the South Branch (Lampland 1912). PA_{ST}: Position angle of the Sunward Tail (Lampland 1912). L_{ST}: Projected length of the Sunward Tail (Lampland 1912). Δt: times of ejection of the dust composing the Neck-Line (days related to perihelion): the former value refers to $1-\mu=0$, the latter to $1-\mu=0.07$

No.	UT	Δ	r	λ	v	PA_{RV}	PA_{SB}	PA_{ST}	L_{ST}	Δt
13	28.089	1.17	0.43	20°.2	114°.0	32°.1	63°.9	244°	10′	−2.8 − −3.4
19	29.089	1.21	0.47	20°.0	116°.5	30°.6	61°.4	241°	10′	−2.7 − −3.2
21	30.084	1.25	0.50	19°.8	118°.6	29°.2	60°.5	241°	10′	−2.5 − −3.0

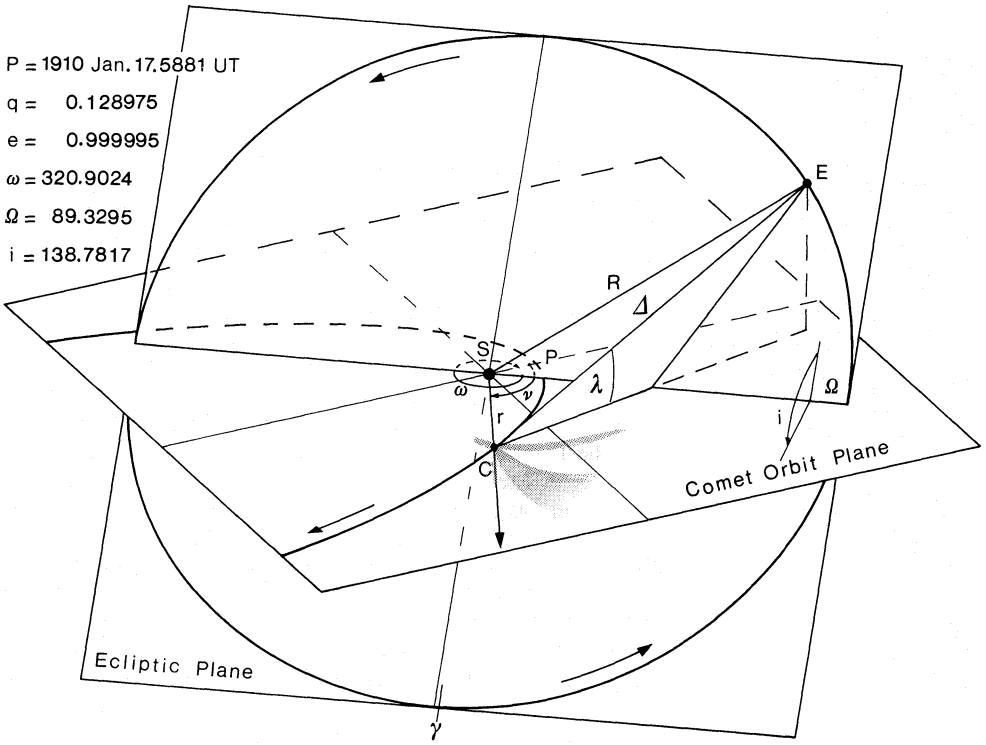

Fig. 1. Earth-Sun-Comet geometry. The diagram refers to the date of the first observation (Plate 13). However it is representative also of the other two observations. E, S, and C denote the position of Earth, Sun and Comet nucleus, whereas P marks the perihelion point of the comet orbit. The shaded image represents the comet tail with its South Branch and related sunward extension. It is slightly oversized for illustrative purposes. The orbital elements at the upper left corner are taken from Marsden (1982). See Table 1 for the values of Δ, r, v, and λ

visible. However the reality of this feature cannot be questioned, because Lampland himself describes this feature as prominent and reports the antitail length and orientation measured on the original plates. The streamer and the spike are much wider than in the cases of C/1970II and C/1986III, and this fact is explained, within the NLS model, by the much higher Earth latitude on the comet orbital plane. The dots along the streamer mark the Neck-Line position computed following the procedure described by Pansecchi et al. (1987).

Although Lampland's images were unfiltered, the large aberration angle of the streamer allows us to exclude an explanation in terms of ion ray (which was possible, although very improbable, for C/1970II and C/1986III). Similarly, due to the high λ values, we do not find a synchronic pile-up sufficient to explain the sharp south border of the dust tail. On the other hand, from Table 1 we see that the dust of the streamer in all three images was ejected during about the same time interval, so that the fit by itself cannot rule out an explanation based on an outburst occurring ≈ 3 days before perihelion. However we point out that only the NLS model gives a natural explanation of both the streamer and the real antitail.

An interesting characteristic of this fit is that, close to the nucleus, the computed dots are close to the brightness maximum of the streamer, whereas far from the nucleus they mark the edge rather than the streamer axis. To explain this fact and to check whether an NLS can also be detected when λ is high, we computed Monte-Carlo simulations of the three dust tails [following the procedure described by Fulle (1989)], which are shown in Fig. 3 (on the assumption of isotropic dust ejection) and in Fig. 4 (on the assumption of anisotropic dust ejection).

These simulations were computed considering the keplerian motion of $\mathcal{N}_t \times \mathcal{N}_\mu \times \mathcal{N}_s$ dust grains, with $\mathcal{N}_t = 72$ samples uniformly distributed in the comet orbit true anomaly interval $-105° < v < +110°$, $\mathcal{N}_\mu = 200$ samples uniformly distributed in the modified size interval $0.001 < 1-\mu < 2.4$ ($1-\mu$ is the solar radiation pressure force expressed in solar gravitational force units, and is inversely proportional to the dust diameter d), and $\mathcal{N}_s = 143$ (spherical shells, Fig. 3) or $\mathcal{N}_s = 66$ (Sun-faced hemi-

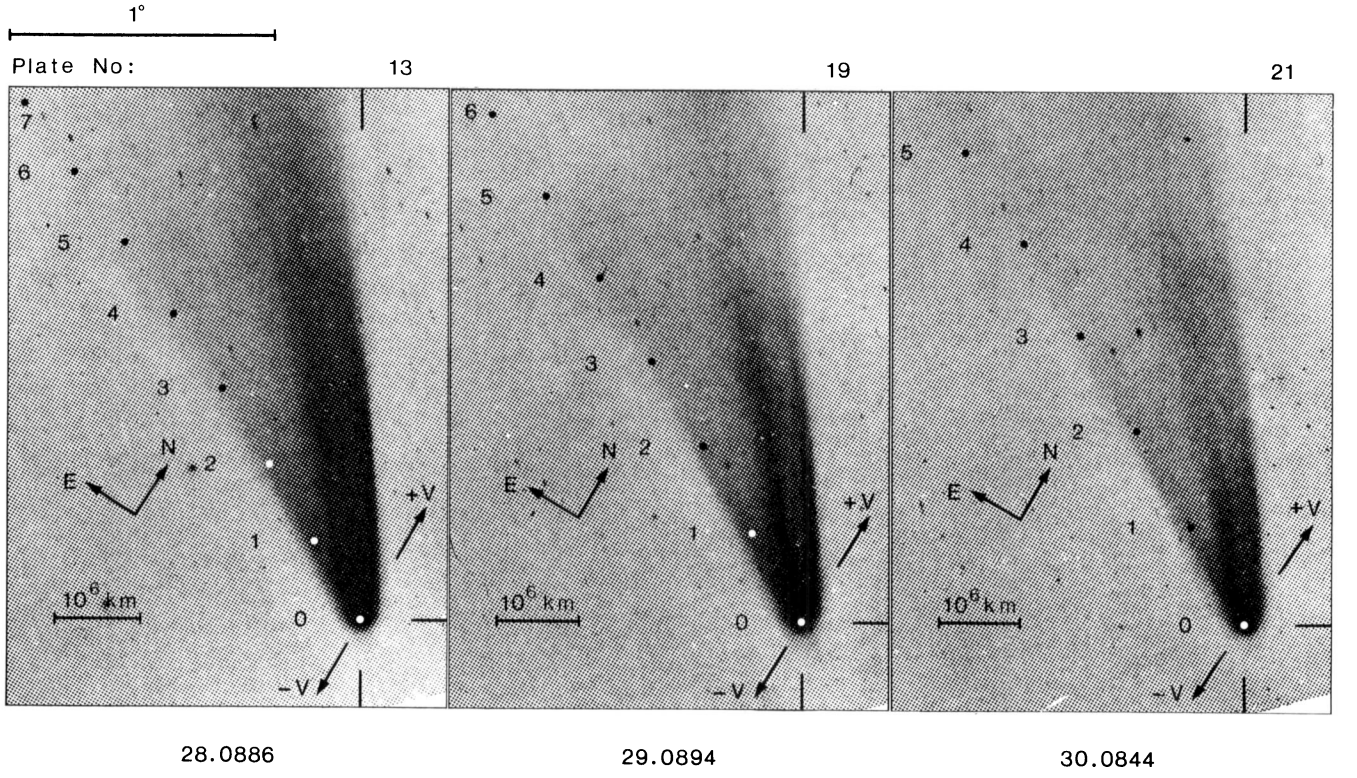

Fig. 2. Partial and enlarged reproduction of the published Lowell Observatory photographs. Solid dots (black or white, depending on the background) mark the computed positions of the Neck-Line for zero ejection velocity, labeled by the related value of $(1-\mu)\times 10^2$. Arrows N, E, +V and −V indicate the direction to the North and to the East through the comet nucleus, and the direction of the sky projection of the comet positive and negative velocity vector, repectively. Vertical segments denote the sky projection of the Sun-Comet radius vector and its prolongation (the M axis of the rectangular coordinate system with origin in the comet nucleus). Plate No. refers to the original Lowell Observatory classification

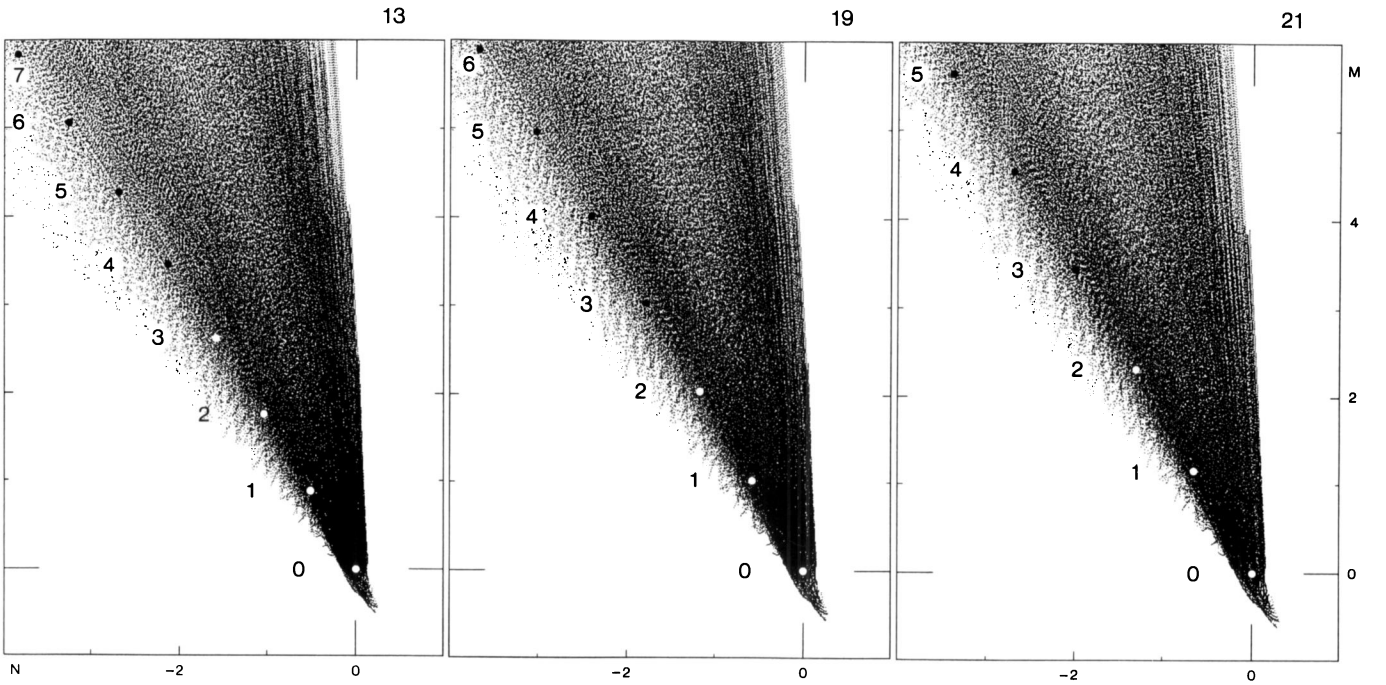

Fig. 3. Numerical simulations of the images shown in Fig. 1 for isotropic dust ejection. Solid dots (black or white, depending on the background) mark the computed positions of the Neck-Line for zero ejection velocity, labeled by the related value of $(1-\mu)\times 10^2$. The M axis is the prolonged projected radius vector, the length unit is 10^6 km. The images are labeled by the original Lowell Observatory classification number

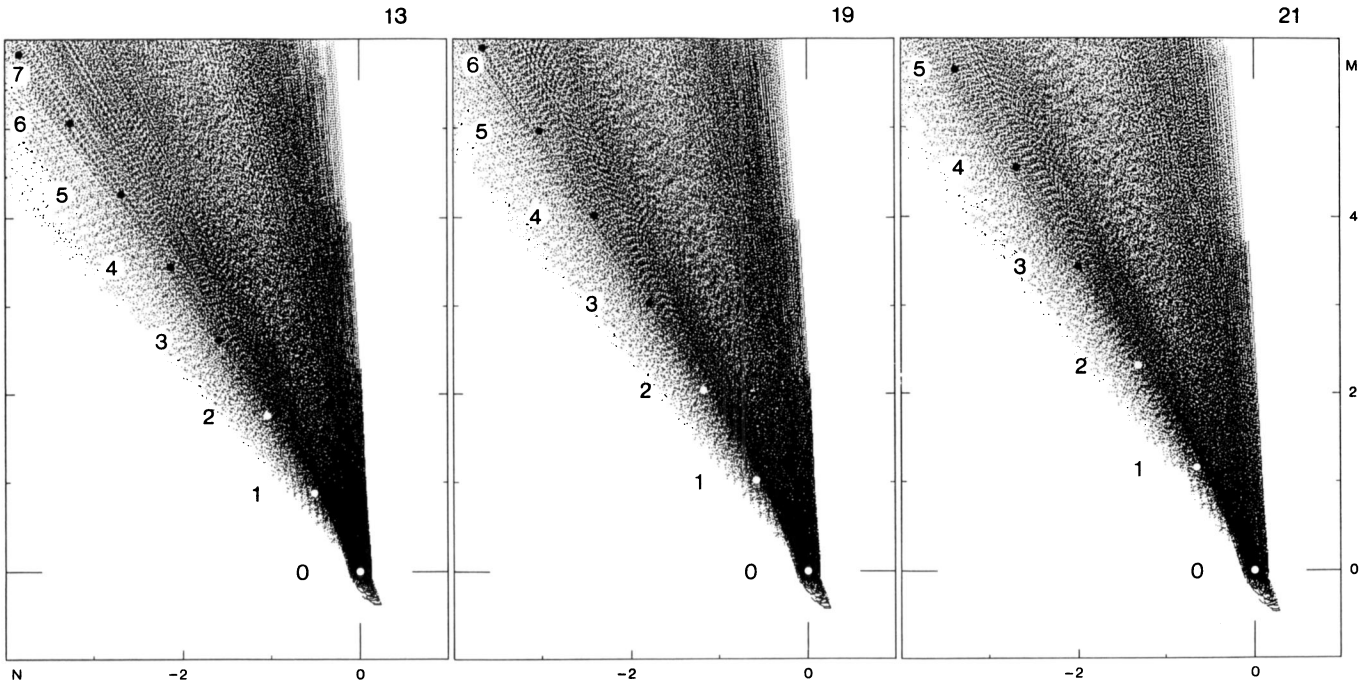

Fig. 4. Numerical simulations of the images shown in Fig. 1 for anisotropic dust ejection. Solid dots (black or white, depending on the background) mark the computed positions of the Neck-Line for zero ejection velocity, labeled by the related value of $(1-\mu)\times 10^2$. The M axis is the prolonged projected radius vector, the length unit is 10^6 km. The images are labeled by the original Lowell Observatory classification number

Table 2. Parameters of the Neck-Line Structures. Comet: the symbol is related to Fig. 5. UT: time of mid-exposure. r: pre-perihelion Sun-Comet distance at which the NLS dust was released (AU). a, b: inverse of the major and minor semiaxes of the isotachies (s^{-1}). s: length parameter of the Neck-Line (cm). Ω_τ: position angle of the major axis of the isotachies with respect to the prolonged radius vector. $\Omega_\tau+\Omega_\mu$: position angle of the Neck-Line with respect to the prolonged radius vector. L: observed projected length of the sunward spike (10^6 km)

Comet	UT	r	a	b	s	Ω_τ	Ω_μ	L
1910I	Jan 28.09	0.18	$38.2\ 10^{-8}$	$3.4\ 10^{-6}$	$1.03\ 10^{13}$	+25°9	+4°3	0.5
○	Jan 29.09	0.18	$34.4\ 10^{-8}$	$3.3\ 10^{-6}$	$1.19\ 10^{13}$	+26°0	+3°5	0.5
	Jan 30.08	0.18	$31.5\ 10^{-8}$	$3.2\ 10^{-6}$	$1.34\ 10^{13}$	+26°2	+3°0	0.5
1970II	May 5.07	1.04	$6.16\ 10^{-8}$	$2.5\ 10^{-6}$	$2.40\ 10^{13}$	− 0°09	−0°02	0.4
□	May 7.05	1.00	$6.02\ 10^{-8}$	$5.9\ 10^{-6}$	$2.54\ 10^{13}$	+ 2°01	+0°32	0.3
	May 8.05	0.99	$5.95\ 10^{-8}$	$4.3\ 10^{-6}$	$2.60\ 10^{13}$	+ 3°04	+0°45	0.5
1986III	May 11.38	0.86	$3.82\ 10^{-8}$	$3.4\ 10^{-6}$	$4.94\ 10^{13}$	+ 4°14	+0°31	0.7
△	Jun 2.38	0.80	$3.23\ 10^{-8}$	$3.2\ 10^{-6}$	$6.24\ 10^{13}$	− 4°14	−0°26	1.0
	Jun 26.35	0.76	$2.74\ 10^{-8}$	$1.5\ 10^{-6}$	$7.78\ 10^{13}$	− 9°4	−0°4	1.4

spherical shells, Fig. 4) samples uniformly distributed on each dust shell. All the models show that only the largest particles (for which $1-\mu\approx 0.001$) are projected into the antitail.

The dust velocity was assumed $v(t,1-\mu)=v(t)\,(1-\mu)^{1/6}$, with $v(t)$ increasing from 0.3 to 0.8 km s^{-1} for $-105°<\nu<-70°$, $v(\nu)=0.8$ km s^{-1} for $-70°<\nu<0°$ and $v(t)$ decreasing from 0.8 to 0.6 km s^{-1} for $0°<\nu<+110°$. The dust loss rate and the modified size distribution $f(t,1-\mu)$ were assumed to be constant. A constant $f(1-\mu)$ corresponds to a differential size distribution $g(d)=d^{-4}$, because $f(1-\mu)$ is weighted by the square of the size. The assumption of a more realistic distribution $g(d)=d^{-3.5}$ does not introduce appreciable changes in our dust tail models, which show that the outburst hypothesis is not necessary to explain the streamer, and that a NLS can be detected also when the Earth is far from the comet orbital plane.

Other simulations computed with a dust velocity $v(t,1-\mu)=v(t)\,(1-\mu)^{1/2}$ give fits of lower quality than those shown in Figs. 3 and 4. In fact the $(1-\mu)^{1/2}$-dependence implies a lower velocity of the large particles of the antitail, and a larger velocity of the small particles of the tail. Therefore the dust tail becomes wider than the observed one and the antitail shorter, so short to lie entirely in the coma. Also the NLS becomes shorter,

because the dust shell sizes fastly increase going outward from the nucleus, so that the shell overlap does not allow to build up a detectable South Branch.

We point out that the real images are better reconstructed by isotropic ejections (Fig. 3), and that in both the reconstructions the Neck-Line is not the locus of maximum brightness, but is close to the edge of the streamer, as really observed. This fact clearly shows that, when λ is high, the photometric behaviour of an NLS is strongly influenced also by the collapsing dust shells, so that the Neck-Line is the photometric axis of the streamer only when $\lambda \approx 0°$.

Similar conclusions are valid for the antitail orientation. The NLS model predicts an angle between the streamer and the antitail of $\pi + \Omega_\mu$ (the NLS parameters are shown in Table 2), whereas the images show a difference of orientation very close to π ($PA_{SB} - PA_{ST}$, see Table 1). The models clearly show that the antitail is not only composed of the isotachies (the completely collapsed shells), but also of the collapsing shells, so that the overlap of collapsing and collapsed shells allows one to obtain a properly oriented broad antitail, as observed. From this discussion it follows that the NLS photometry can give reliable results only when λ is very low, that is when the NLS brightness is effectively scattered only by the dust collapsed on the comet orbital plane.

3. The size dependence of the dust velocity

The length of the sunward spike of Neck-Line Structures gives the most immediate constraint to the size dependence of the dust velocity $v(d)$. In fact, Pansecchi et al. (1987) have shown that the spike length L depends only on the NLS parameters a and s (Table 2), on the velocity at a fixed diameter d and on the power index $u = \partial \log v / \partial \log d$. Since a and s depend on keplerian dynamics only, and therefore cannot be affected by significant uncertainties, the spike length allows us to constrain the dust velocity at a given diameter d:

$$v(d) = \frac{a L \left[\frac{L \varrho d}{s C}\right]^u}{[|u|^{-u/(1+u)} - |u|^{1/(1+u)}]^{1+u}}. \quad (1)$$

The power index u is assumed to be constant over the size range covered by a Neck-Line, and this hypothesis is satisfied for $d > 40\,\mu m$ (Gombosi 1986; Crifo 1987). For these dust diameters the dust bulk density ϱ and the parameter C can be considered constant quantities, $\varrho = 1\,g\,cm^{-3}$, $C = 1.19\ 10^{-4}\,g\,cm^{-2}$ (Burns et al. 1979). In Fig. 5 we plot the dust velocity (for $d = 40\,\mu m$ and $d = 4\,mm$) which is required to obtain a sunward spike of the observed length for the three comets which showed NLS's (Table 2). The noise of the photographic images does not allow the detection of the whole spike, so that the plotted dust velocities should be considered as lower limits only. We point out that such lower limits are in fact lower than the dust velocities obtained by means of the photometry of the NLS of Comet Halley ($v = 0.07\,km\,s^{-1}$ for $d = 4\,mm$, Cremonese & Fulle 1989), which imply longer sunward spikes than the observed ones, and also lower than the dust velocity adopted in our simulations of the Lampland's images ($v = 0.8 \times (0.001)^{1/6}\,km\,s^{-1} = 0.25\,km\,s^{-1}$), which show a sunward spike a bit longer than the observed one.

The NLS photometry has supplied a power index $u \geqq -0.15$ and a velocity value of $\approx 0.1\,km\,s^{-1}$ at $d = 40\,\mu m$ for C/1970II and C/1986III, satisfying the constraints of Fig. 5. Richter & Keller

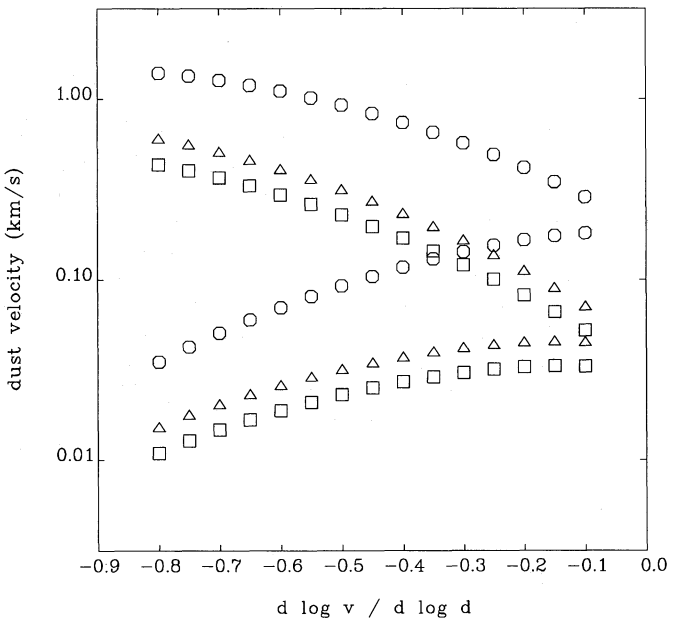

Fig. 5. Constraint on the dust velocity given by the length of the sunward spike. For a given dust velocity power index $\partial \log v / \partial \log d$, the dust velocity for a dust diameter $d = 40\,\mu m$ (higher symbols) or for $d = 4\,mm$ (lower symbols) must be higher than the plotted values. The symbols refer to C/1910I (circles), C/1970II (squares) and C/1986III (triangles, see Table 2)

(1988) interpreted the perspective sunward streamer of Comet Kohoutek 1973XII by means of $u = -0.5$. However this value was assumed as a hypothesis which was not tested on the data. In fact they showed neither the dependence of the results on other values of u, nor the fit of the width of the streamer along its length. Studying these quantities allowed Fulle & Sedmak (1988) and Cremonese & Fulle (1989) to obtain $u \geqq -0.15$ directly from the data.

For $d \geqq 40\,\mu m$ hydrodynamic models of the inner coma give a power index $u = -0.5$. The corresponding velocity for $d = 40\,\mu m$ ($v = 0.10\,km\,s^{-1}$ at $r = 0.75\,AU$ before perihelion) given by Divine et al. (1986) for C/1986III does not satisfy the constraint of Fig. 5. Other models computed after the Halley spacecraft encounters for the fly-by conditions ($r = 0.88\,AU$ after perihelion, Gombosi 1986; Crifo 1987) reach the lower limit, but probably such models would yield lower velocities before perihelion (as for the computations of Divine et al. (1986), $v = 0.10\,km\,s^{-1}$ at $r = 0.75\,AU$ before perihelion, $v = 0.13\,km\,s^{-1}$ at $r = 0.88\,AU$ after), so that the disagreement already obtained between NLS photometry and hydrodynamic models is confirmed by the simple observation of the sunward spike length. We must conclude that actual models of the inner coma cannot explain the observed length of the real antitail of P/Halley. Such inconsistency with observations is much more evident for Comet 1910I, which developed such a long antitail to require much higher dust ejection velocities. Therefore the length of the sunward tail of C/1910I can supply a significant test for the models of dust-gas interaction in the inner coma.

The high dust velocity of the largest particles released by C/1910I has also significant implications for its dust mass loss rate. When we assume that the density of dust in the inner coma is about constant, an increase of the dust velocity is directly reflected into the same increase of the dust loss rate. Since the velocity of $0.2\,km\,s^{-1}$ for millimeter sized particles may be five times higher than the value predicted by usual inner coma models, we obtain a

similar increase of the mass loss rate. Unfortunately it is impossible to obtain absolute calibrations of the Lampland images, so that this conclusion cannot be quantified. We assume that the behaviour of C/1910I was similar to that of well studied bright comets, as Comet Bennett 1970II or West 1976VI, which showed a dust to gas mass ratio of 0.2–0.5 (Ney 1982). Our velocities increase the dust to gas mass ratio to about 2, a value close to that of Comet Halley (McDonnell et al. 1990). For Comet Halley, such high dust to gas ratio was mainly due to the high power index of the size distribution of the largest particles. Our models show that for C/1910I the usual power index -4 is consistent with the available observations, so that the high dust velocity of C/1910I may have introduced in the dust to gas ratio effects similar to those due to the high size distribution power index of C/1986III. More significant tests on our results are prevented by the lack of other quantitative data, which also does not allow us to study possible changes of the size distribution along the sunward spike.

4. Conclusions

The very favourable perspective conditions of the observations of C/1910I (Lampland 1912) allow us to conclude that the most probable explanation of the streamer and of the real antitail of this comet is given by the NLS model. The large aberration angle of the streamer excludes an ion ray interpretation. Numerical simulations show that an outburst ≈ 3 days before perihelion is not necessary to explain the streamer, because it is well reconstructed also with a constant dust loss rate, showing that it can be explained by means of the dust dynamics only. The observation of the antitail further supports these conclusions. However numerical simulations of the real images show that when the Earth is well away from the comet orbital plane, the shape of a NLS depends not only on the dust shells completely collapsed on the comet orbital plane, but also on the collapsing dust shells. This fact explains the residual differences between the NLS model and the observational data and shows that the NLS photometry can give reliable results only when the Earth is close to the comet orbital plane, as occurred for C/1970II and C/1986III.

The Neck-Line Structure photometry yelds the size dependence of the velocity of large dust grains ($u = \partial \log v / \partial \log d$, Fulle & Sedmak 1988; Cremonese & Fulle 1989), while the length of sunward spikes constrains the velocity value at a given dust size. Both the observed size dependence and the spike lengths disagree with actual models of dust gas interaction in the inner coma. The observed power index ($u \approx -0.15$) is significantly higher than that computed by hydrodynamical models of the inner coma ($u = -0.5$, Gombosi 1986; Crifo 1987). The velocities predicted by the inner coma models are systematically lower than the values required to explain the spike lengths. In particular, the length of the sunward spike of C/1910I requires an ejection velocity from the inner coma larger than $0.2\,\mathrm{km\,s^{-1}}$ for millimeter sized grains. The spike length depends only upon the dynamics of the dust grains out of the coma, which is affected by uncertainties by far smaller than those affecting actual inner coma models. Therefore the Neck-Line model can point out significant inconsistencies in actual models of dust-gas interaction. The high dust velocities required by the length of the sunward spikes may have significant effects on the dust loss rate of comets. Therefore further NLS analyses are necessary both to confirm the results obtained for C/1910I by means of the analysis of NLS's of well studied comets, and to solve the theoretic inconsistencies between the results of the NLS model and actual inner coma models.

References

Burns, J.A., Lamy, P.L., Soter, S., 1979, Icarus 40, 1

Cremonese, G., Fulle, M., 1989, Icarus 80, 267

Crifo, J.F., 1987, Symposium on the Diversity and Similarity of Comets ESA SP-278, 399

Divine, N., Fechtig, H., Gombosi, T.I., Hanner, M.S., Keller, H.U., Larson, S.M., Mendis, D.A., Newburn, R.L., Reinhard, R., Sekanina, Z., Yeomans, D.K., 1986, Space Sci. Rev. 43, 1

Fulle, M., 1987, A&A 181, L13

Fulle, M., 1989, A&A 217, 283

Fulle, M., Sedmak, G., 1988, Icarus 74, 383

Gombosi, T.I., 1986, 20th ESLAB Symposium on the Exploration of Halley's Comet ESA SP-250, Vol. 3, 167

Kimura, H., Liu, C.P., 1977, Chinese Astron. 1, 235

Lampland, C.O., 1912, Lowell Obs. Bull. 57, 34

Marsden, B.G., 1982, Catalogue of Cometary Orbits, 4th Ed., Central Bureau for Astronomical Telegrams, Cambridge

McDonnell, J.A.M., Green, S.F., Nappo, S., Pankiewicz, G.S., Perry, C.H., Zarnecki, J.C., 1990, Icarus (in press)

Ney, E.P., 1982, in Comets, ed. L.L. Wilkening, The University of Arizona Press, Tucson, p. 323

Pansecchi, L., Fulle, M., Sedmak, G., 1987, A&A 176, 358

Richter, K., Keller, H.U., 1988, A&A 206, 136

Sekanina, Z., 1974, Sky Tel. 47, 374